Geophysical Journal International

Geophys. J. Int. (2011) **187,** 1699–1707 doi: 10.1111/j.1365-246X.2011.05229.x

An irregular lattice method for elastic wave propagation

Gareth S. O'Brien and Christopher J. Bean

School of Geological Sciences, University College Dublin, Belfield, Dublin 4, Ireland. E-mail: gareth.obrien@ucd.ie

Accepted 2011 September 9. Received 2011 September 9; in original form 2011 April 8

SUMMARY

Lattice methods are a class of numerical scheme which represent a medium as a connection of interacting nodes or particles. In the case of modelling seismic wave propagation, the interaction term is determined from Hooke's Law including a bond-bending term. This approach has been shown to model isotropic seismic wave propagation in an elastic or viscoelastic medium by selecting the appropriate underlying lattice structure. To predetermine the material constants, this methodology has been restricted to regular grids, hexagonal or square in 2-D or cubic in 3-D. Here, we present a method for isotropic elastic wave propagation where we can remove this lattice restriction. The methodology is outlined and a relationship between the elastic material properties and an irregular lattice geometry are derived. The numerical method is compared with an analytical solution for wave propagation in an infinite homogeneous body along with comparing the method with a numerical solution for a layered elastic medium. The dispersion properties of this method are derived from a plane wave analysis showing the scheme is more dispersive than a regular lattice method. Therefore, the computational costs of using an irregular lattice are higher. However, by removing the regular lattice structure the anisotropic nature of fracture propagation in such methods can be removed.

Key words: Numerical solutions; Computational seismology; Wave propagation.

1 INTRODUCTION

The physical theory behind seismic wave propagation is well understood and seismic waves can be modelled as waves propagating through geological materials with different rheologies, such as elastic, viscoelastic or poroelastic media, see Aki & Richards (2002). The wave equation can be solved in a variety of ways, for example, analytical solutions for simple models (e.g. Carcione 2007), ray tracing approximations (e.g. Brokešová 2006), finite-difference methods (e.g. Virieux 1986) and spectral element methods (e.g. Komatitsch & Vilotte 1998). However, because the Earth is heterogeneous at all scales, analytical solutions to the elastic, viscoelastic and poroelastic wave equations are very limited in their applicability to geological problems and numerical solutions are becoming common tools used by seismologist to study the Earth's interior.

Seismic wave propagation is governed by a wave equation. This wave equation is a continuum equation in which the variables representing material properties are continuous within the medium. These variables are averaged over a representative elemental volume (REV). The REV is defined such that regardless where in space the volume is placed the averages obtained are statistically meaningful. The averages obtained must be independent of the REV size and the REV must be smaller than the overall size of the system. Once average variables are defined, the equations of state are derived from conservation laws and momentum and force balance equations. The most common techniques for solving seismic wave propagation utilise the continuum approach. An alternative approach to continuum mechanics is to use a discrete method. These discrete methods do not solve continuum equations by any approximate numerical method. Instead, the aim is to replicate the underlying physics at a 'microscopic scale' employing discrete micromechanical interaction rules between discrete material particles or nodes. In most cases, by assuming some form of linearization or approximate global behaviour, a macroscopic continuum equation can be derived from the local interactions. It should be stressed that the schemes are not solving the macroscopic continuum equation but this macroscopic behaviour arises through the local mesoscopic interactions. A class of discrete methods using particle–particle mechanical interactions (e.g. Hooke's law) are capable of modelling seismic waves propagating in a heterogeneous Earth model. These discrete particle–particle methods, also called elastic lattice methods (ELM), originate from solid-state physics models of crystalline materials (Hoover *et al*. 1974). As these schemes solely rely on particle–particle mechanical interactions, complex boundary conditions can be readily implemented which makes them ideally suited to geological processes. One of the first discrete particle methods was developed by Cundall & Strack (1979) for granular material and is a mesh-free method. These mesh-free or irregular lattices have been primarily used to study static deformation and fracturing. They are not suitable for wave propagation as the methods have to be calibrated so the *P*-wave velocity and Poisson's ratio can be found. The *P*-wave velocity may also be heterogeneous and anisotropic due to the irregular lattice.

Regular lattices have been used to overcome the difficulties in deriving material constants and have been used to model seismic waves by several authors but they have lost the advantage of a

mesh-free grid. Monette & Anderson (1994) used hexagonal and square lattices to study brittle failure but did not apply the method to seismic wave propagation. Toomey & Bean (2000) used a hexagonal arrangement of particles to model seismic wave propagation in a Poisson solid. Along with verifying that their discrete particle method compares well with a finite-difference solution, they also compared the method to analytical results for static deformatio, (Toomey *et al*. 2002). They also modelled wave propagation across fractures and this work has been extended recently by Möllhoff & Bean (2008). Del Valle-Garcia & Sanchez-Sesma (2003) used a similar method, but included a bond-bending force term which removes the restriction on a Poisson's ratio of 0.25 to model seismic waves including Rayleigh waves. O'Brien & Bean (2004) used a cubic lattice with a bond-bending term to model 3-D wave propagation in the presence of complex topography. The numerical accuracy and computational cost of this methodology has been examined by O'Brien *et al*. (2009). The above methods were restricted to an elastic rheology but by including damping terms the rheology can be changed. O'Brien (2008) applied the discrete particle methods to viscoelastic wave propagation by including dashpots and springs in series. These discrete methods offer an alternative method for modelling seismic wave propagation in complex media. As stated earlier, including heterogeneity is vital in any geological application of wave propagation, therefore using irregular grids or mesh-free grids is highly advantageous. Because the above particle methods for wave propagation are restricted to a regular grid they lose this advantage. In this paper, we will present a discrete lattice method for a mesh-free or irregular lattice. Here, we only consider a 2-D lattice but the same principles hold for a 3-D method. The restriction on using a regular lattice is removed by including many nearest neighbours and is discussed in Section 2. The dispersion characteristics are derived and the scheme is compared with an analytical expression for wave propagation in a 2-D homogenous infinite medium. Irregular grid results are also compared with results from a spectral element method (Komatitsch & Vilotte 1998) for a more complex model.

2 DISCRETE LATTICE METHOD

The lattice method considers the medium to be composed of nodes or particles which are linked to a number of neighbours by elastic springs, in this case a 2-D lattice (Fig. 1). The number of neighbours and node geometry determines the macroscopic behaviour of the system. As stated earlier, regular lattices have been studied previously so we will restrict the discussion to irregular or mesh-free geometries. We consider a lattice where the nodes are distributed randomly in space. However, the derivation that follows equally applies to any geometrical arrangement. The goal is then to determine the macroscopic behaviour of the system and relate it to the continuum elastic wave equation. This will allow us to define material properties and therefore simulate seismic waves in our known geological model. Again, we stress that the method is based on solving the equations of motion of the particles/nodes not the continuum wave equation. The elastic energy E_i for a node i surrounded by N neighbours is expressed as (Arbabi & Sahimi 1988)

$$E_i = \frac{1}{2}\sum_{n=1}^{N} K_{in}\left(|\mathbf{r}_{in}| - |\mathbf{r}^{\mathrm{o}}_{in}|\right)^2 + \frac{1}{2}\sum_{nim} G_{nim}\left(\mathrm{Cos}\,\theta_{nim} - \mathrm{Cos}\,\theta^{\mathrm{o}}_{nim}\right)^2, \quad (1)$$

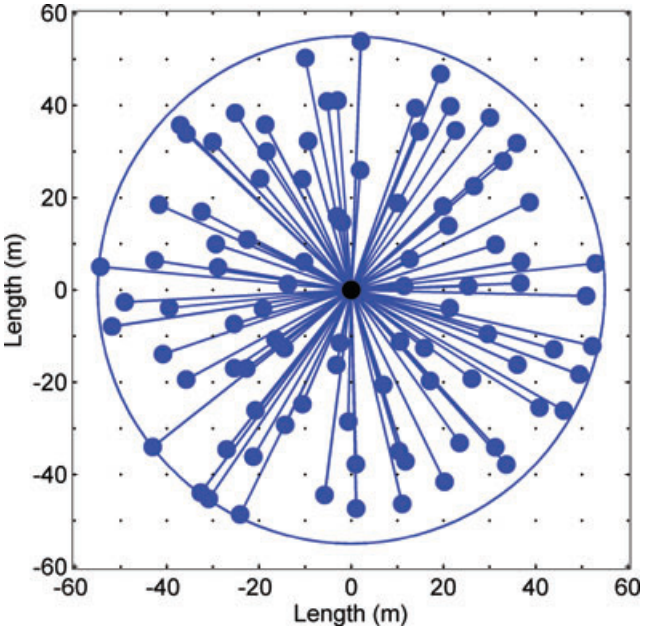

Figure 1. A lattice method consists of particles (filled circles) connected by springs shown as solid lines. The particle here is connected to 96 other particles with the outer bound of the interaction zone shown by the solid line. By increasing the number of neighbours irregular lattices such as the distribution shown here can be used to model isotropic elastic wave propagation.

where K_{in} is the elastic spring constant between nodes i and n, G_{nim} is the bond-bending constant and θ_{nim} is the angle between particles nim with node i being the apex of the angle. $\mathbf{r}_{in}$ is the vector connecting nodes $\mathbf{x}_i$ and $\mathbf{x}_n$ with a superscript $^{\mathrm{o}}$ representing the undistorted lattice. The energy density Φ is the total energy stored in each spring divided by the total volume and can be written as

$$\Phi = \frac{1}{4}\sum_{in=1}^{N} K_{in}\left(|\mathbf{r}_{in}| - |\mathbf{r}^{\mathrm{o}}_{in}|\right)^2 + \frac{1}{2}\sum_{nim} G_{nim}\left(\mathrm{Cos}\,\theta_{nim} - \mathrm{Cos}\,\theta^{\mathrm{o}}_{nim}\right)^2. \quad (2)$$

To derive the macroscopic properties of the system, we assume the deformation is small and hence restricts the analysis to linear elasticity. However, this assumption only applies when deriving the macroscopic behaviour as the equations of motion of the particles are not restricted to linear elasticity. Linearising eq. (2) yields

$$\Phi = \frac{1}{4}\sum_{n=1}^{N} \frac{K_{in}}{|\mathbf{r}_{in}|^2}\left(\mathbf{u}_{in}\cdot\mathbf{r}_{in}\right)^2 + \frac{1}{2}\sum_{nim} G_{nim}\left(\frac{\mathbf{u}_{in}\cdot\mathbf{s}_{in}}{|\mathbf{r}_{in}|^2} - \frac{\mathbf{u}_{im}\cdot\mathbf{s}_{im}}{|\mathbf{r}_{im}|^2}\right)^2, \quad (3)$$

where the displacement $\mathbf{u}_{in}$ is the displacement vector ($\mathbf{u}_i$–$\mathbf{u}_n$) and

$$s_{in} \equiv (s_x, s_y) = \left(\frac{x_{in}}{|\mathbf{r}_{in}|}, \frac{-y_{in}}{|\mathbf{r}_{in}|}\right). \quad (4)$$

Substituting the x- and y-displacement given by

$$u_{in} = x_n\frac{\partial u}{\partial x} + y_n\frac{\partial u}{\partial y} \quad (5)$$

$$v_{in} = x_n\frac{\partial v}{\partial x} + y_n\frac{\partial v}{\partial y} \quad (6)$$

into the linear elastic density (eq. 3) gives

$$\Phi = \frac{1}{4}\sum_{n=1}^{N}\frac{K_{ij}}{|\mathbf{r}_{in}|^2}\left(x_{in}^2\frac{\partial u}{dx}+x_{in}y_{in}\frac{\partial u}{dy}+x_{in}y_{in}\frac{\partial v}{dx}+y_{in}^2\frac{\partial v}{dy}\right)^2 + \frac{1}{2}\sum_{nim}G_{nim}\left(a_{nim}\frac{\partial u}{dx}+b_{nim}\frac{\partial u}{dy}-c_{nim}\frac{\partial v}{dx}-a_{nim}\frac{\partial v}{dy}\right)^2, \tag{7}$$

where

$$a_{nim} = \frac{x_{in}y_{in}}{|\mathbf{r}_{in}|} - \frac{x_{im}y_{im}}{|\mathbf{r}_{im}|},$$
$$b_{nim} = \frac{y_{in}y_{in}}{|\mathbf{r}_{in}|} - \frac{y_{im}y_{im}}{|\mathbf{r}_{im}|},$$
$$c_{nim} = \frac{x_{in}x_{in}}{|\mathbf{r}_{in}|} - \frac{y_{im}y_{im}}{|\mathbf{r}_{im}|}. \tag{8}$$

The elastic energy density of an isotropic elastic continuum (Landau & Lifshitz 1986) can be written in terms of the Lamé constants as follows:

$$\Phi = \left(\frac{\lambda}{2}+\mu\right)\left(\frac{\partial u}{\partial x}\right)^2 + \left(\frac{\lambda}{2}+\mu\right)\left(\frac{\partial v}{\partial y}\right)^2 + \lambda\left(\frac{\partial u}{\partial x}\right)\left(\frac{\partial v}{\partial y}\right) + \frac{\mu}{2}\left(\frac{\partial u}{\partial y}+\frac{\partial v}{\partial x}\right)^2. \tag{9}$$

Expanding eq. (7) and comparing terms with the continuum energy density yields, the set of 10 equations relating the lattice geometry, number of neighbours and the spring and bond bending constants to the macroscopic material properties.

$$\sum_n \frac{K_{in}x_{in}^4}{4|r_{in}|^2} + \sum_{nim}\frac{G_{nim}a_{nim}^2}{2} = \frac{\lambda}{2}+\mu,$$
$$\sum_n \frac{K_{in}y_{in}^4}{4|r_{in}|^2} + \sum_{nim}\frac{G_{nim}a_{nim}^2}{2} = \frac{\lambda}{2}+\mu,$$
$$\sum_n \frac{K_{in}x_{in}^2y_{in}^2}{4|r_{in}|^2} - \sum_{nim}\frac{G_{nim}a_{nim}^2}{2} = \frac{\lambda}{2},$$
$$\sum_n \frac{K_{in}x_{in}^2y_{in}^2}{4|r_{in}|^2} + \sum_{nim}\frac{G_{nim}b_{nim}^2}{2} = \frac{\mu}{2},$$
$$\sum_n \frac{K_{in}x_{in}^2y_{in}^2}{4|r_{in}|^2} + \sum_{nim}\frac{G_{nim}c_{nim}^2}{2} = \frac{\mu}{2},$$
$$\sum_n \frac{K_{in}x_{in}^2y_{in}^2}{4|r_{in}|^2} - \sum_{nim}\frac{G_{nim}b_{nim}c_{nim}}{2} = \frac{\mu}{2},$$
$$\sum_n \frac{K_{in}x_{in}^3y_{in}}{4|r_{in}|^2} + \sum_{nim}\frac{G_{nim}a_{nim}b_{nim}}{2} = 0,$$
$$\sum_n \frac{K_{in}x_{in}^3y_{in}}{4|r_{in}|^2} + \sum_{nim}\frac{G_{nim}a_{nim}c_{nim}}{2} = 0,$$
$$\sum_n \frac{K_{in}x_{in}y_{in}^3}{4|r_{in}|^2} + \sum_{nim}\frac{G_{nim}a_{nim}b_{nim}}{2} = 0,$$
$$\sum_n \frac{K_{in}x_{in}y_{in}^3}{4|r_{in}|^2} + \sum_{nim}\frac{G_{nim}a_{nim}c_{nim}}{2} = 0. \tag{10}$$

Therefore, if the lattice method is to model an isotropic elastic continuum in the limit of linear elasticity, the set of 10 equations in (10) above must be satisfied. Several different strategies can be employed to solve this system of equations. By using a regular lattice, the equations can easily be solved for a fixed set of spring and bond-bending constants. A solution of this type for a hexagonal and square lattice is given in Monette & Anderson (1992) and a solution for a cubic lattice is given in O'Brien & Bean (2004). Another possible strategy is to remove the restriction on the regular lattice. This then requires that each spring and bond-bending constant becomes a free parameter and the set of equations for every node must be solved for every K_{in} and G_{nim}. This leads to an inversion problem that can be intractable. We will not address this strategy but highlight two problems. First, it maybe that no solution may exist and secondly and more likely, because K_{in} is a free parameter the solution will involve negative spring constants which are physically unrealistic.

The approach set out later is to keep the advantage of a mesh-free gird while not having to solve the inversion problem. To do this we assume the spring constants K are fixed for every lattice link. For the system of equations to be consistent under this assumption, eq. (11) must hold.

$$\sum_n \frac{x_{in}^4}{|r_{in}|^2} = \sum_n \frac{y_{in}^4}{|r_{in}|^2} = \frac{1}{3}\sum_n \frac{x_{in}^2y_{in}^2}{|r_{in}|^2},$$
$$\sum_{nim} a_{nim}^2 = \sum_{nim} b_{nim}^2 = \sum_{nim} c_{nim}^2 = -\sum_{nim} b_{nim}c_{nim},$$
$$\sum_n \frac{x_{in}^3y_{in}}{|r_{in}|^2} = \sum_n \frac{x_{in}y_{in}^3}{|r_{in}|^2} = 0,$$
$$\sum_{nim} a_{nim}c_{nim} = \sum_{nim} a_{nim}b_{nim} = 0. \tag{11}$$

Consider a circle with radius R centred on the origin (Fig. 1). If we randomly populate the circle with particles and calculate the sums in eq. (11) using the positions, we can see that for a large enough sample the equations in (11) hold. To show why this is true, as the number of particles increases we can replace the sums with the integral equations. The first line of equations in (11) becomes

$$\sum_n \frac{x_{in}^4}{|r_{in}|^2} \to \frac{1}{p(r)}\frac{1}{p(\theta)}\int_0^R \mathrm{d}r\int_0^{2\pi} r^2\,\mathrm{Cos}^4(\theta)\,\mathrm{d}\theta = \frac{R^2}{8},$$

$$\sum_n \frac{y_{in}^4}{|r_{in}|^2} \to \frac{1}{p(r)}\frac{1}{p(\theta)}\int_0^R \mathrm{d}r\int_0^{2\pi} r^2\mathrm{Sin}^4(\theta)\,\mathrm{d}\theta = \frac{R^2}{8},$$

$$\sum_n \frac{x_{in}^2y_{in}^2}{|r_{in}|^2} \to \frac{1}{p(r)}\frac{1}{p(\theta)}\int_0^R \mathrm{d}r\int_0^{2\pi} r^2\mathrm{Cos}^2(\theta)\mathrm{Sin}^2(\theta)\,\mathrm{d}\theta = \frac{R^2}{24},$$

$$\sum_n \frac{x_{in}y_{in}^3}{|r_{in}|^2} \to \frac{1}{p(r)}\frac{1}{p(\theta)}\int_0^R \mathrm{d}r\int_0^{2\pi} r^2\mathrm{Cos}(\theta)\mathrm{Sin}^3(\theta)\,\mathrm{d}\theta = 0,$$

$$\sum_n \frac{x_{in}^3y_{in}}{|r_{in}|^2} \to \frac{1}{p(r)}\frac{1}{p(\theta)}\int_0^R \mathrm{d}r\int_0^{2\pi} r^2\mathrm{Cos}^3(\theta)\mathrm{Sin}(\theta)\,\mathrm{d}\theta = 0,$$

$$p(r) = R \quad p(\theta) = 2\pi\,, \tag{12}$$

where the Cartesian coordinates have been transformed to polar coordinates. The probability density functions $p(r)$ and $p(\theta)$ are for a uniform distribution. From the equations it can be clearly seen that as the number of neighbours tends to infinity the required relationships hold. For the second set of equations in the set (11), a similar derivation applies.

$$\sum_n a_{nim}^2 \to \frac{1}{p(r_n)}\frac{1}{p(\theta_n)}\frac{1}{p(r_m)}\frac{1}{p(\theta_m)}\int_0^R \mathrm{d}r_m\int_0^R \mathrm{d}r_n\int_0^{2\pi}\mathrm{d}\theta_m \int_0^{2\pi} F(\theta_n,\theta_m)\,\mathrm{d}\theta_n = \frac{3}{16}. \tag{13}$$

$$F(\theta_n, \theta_m) = (1 - \mathrm{Cos}(\theta_m)\mathrm{Cos}(\theta_n) - \mathrm{Sin}(\theta_m)\mathrm{Sin}(\theta_n)) \\ (\mathrm{Cos}(\theta_m)\mathrm{Cos}(\theta_n) + 1 + \mathrm{Sin}(\theta_m)\mathrm{Sin}(\theta_n)) \\ (\mathrm{Cos}(\theta_m)\mathrm{Sin}(\theta_m) - \mathrm{Cos}(\theta_n)\mathrm{Sin}(\theta_n))^2 . \tag{14}$$

Similarly, the same transformation to an integral equation can be performed for b_{nim}^2, c_{nim}^2 and $a_{nim}b_{nim}$, $a_{nim}c_{nim}$ and $b_{nim}c_{nim}$, which satisfy the remaining equations. So by assuming the number of neighbours distributed randomly inside a circle of radius R tends to infinity, the elastic lattice method tends to an isotropic elastic continuum. A large number of particles are required to satisfy the integral solutions, however, the absolute value of the integral solution is not required only the relative values between the set of equations. These relative values are attained with enough accuracy with a minimum of ∼40 neighbours. Therefore, calculating the spring and bond bending constants using eqs (15) and (16) allows the method to reproduce an isotropic continuum using a computationally feasible number of particles

$$K_{in} = \frac{3}{X_{in}}\left(\frac{\lambda_i + \lambda_n + \mu_i + \mu_n}{2}\right), \tag{15}$$

$$G_{nim} = \frac{0.5}{A_{nim}}\left(\frac{-\lambda_i - \lambda_n + \mu_i + \mu_n}{2}\right), \tag{16}$$

where X_{in} and A_{nim} are the respective sums over the neighbour positions in the first equation in eq. (10). The derivation above is not restricted to particles distributed randomly inside a circle, as long as eq. (11) holds for any lattice structure the system will behave as an isotropic elastic body. The derivation above was used to illustrate why the system tends to an elastic continuum.

In practice, the force acting on each spring is calculated at each time step using eq. (17) and the new position of the lattice nodes and node velocities are updated using the velocity-Verlet numerical integration scheme (Allen & Tildesley 1987).

$$\mathbf{F}^{t+\Delta t} = \sum_{in=1}^{N} K_{in}\left(|\mathbf{r}_{in}|^t - |\mathbf{r}_{in}^o|\right)\cdot\mathbf{r}_{in}^t + \sum_{nim} G_{nim}\left(\frac{\mathbf{u}_{\mathbf{ij}}^t}{|\mathbf{r}_{in}|^2}\right), \tag{17}$$

The velocity-Verlet integration scheme is symplectic and time reversible, which implies good stability. For numerical stability, the Courant condition applies,

$$\Delta t < \frac{\Delta x}{V_{\max}}, \tag{18}$$

where Δt is the time step, Δx is the minimum distance between two nodes and $V_{\max}$ is the maximum wave velocity. Heterogeneity can be incorporated into the model by changing the elastic spring constants on each spring. Topography is introduced by simply removing any particles above the required free surface. This imposes an implicit vacuum free-surface boundary condition. Previous lattice methods for wave propagation have solely relied on regular lattices to solve eq. (10). By arbitrarily increasing the number of neighbours and keeping the spring constant K and the bond-bending constant G fixed, the restriction on the regular lattice is removed. This is true if and only if the set of equations in eq. (11) hold. Whether this set of equations hold will depend on including a large enough number of neighbours over a large enough circle of influence.

3 DISPERSION ANALYSIS

Before we test the method outlined above against analytical and numerical solutions we first derive the dispersion relationship using von Neumann analysis. The velocity-Verlet scheme for the particle motion is given in eqs (19)–(22).

$$\mathbf{u}^{t+\Delta t} = \mathbf{u}^t + \Delta t\mathbf{v}^t + \frac{\Delta t^2\mathbf{F}^t}{2\rho}, \tag{19}$$

$$\mathbf{v}^{t+\Delta t/2} = \mathbf{v}^t + \frac{\Delta t^2\mathbf{F}^t}{2\rho}, \tag{20}$$

$$\mathbf{F}^{t+\Delta t} = \sum_{in=1}^{N} K_{in}\left(|\mathbf{r}_{in}|^t - |\mathbf{r}_{in}^o|\right)\cdot\mathbf{r}_{in}^t + \sum_{nim} G_{nim}\left(\frac{\mathbf{u}_{\mathbf{ij}}^t}{|\mathbf{r}_{in}|^2}\right), \tag{21}$$

$$\mathbf{v}^{t+\Delta t} = \mathbf{v}^{t+\Delta t/2} + \frac{\Delta t^2\mathbf{F}^{t+\Delta t}}{2\rho}. \tag{22}$$

The scheme is second order in time and can be approximated by substituting eqs (20) and (22) into eq. (19).

$$\mathbf{u}^{t+\Delta t} = 2\mathbf{u}^t - \mathbf{u}^{t-\Delta t} + \frac{\Delta t^2\mathbf{F}^t}{\rho}. \tag{23}$$

Letting the displacement be a plane wave

$$\mathbf{u} \equiv \left(u_0 e^{-i\omega t + i\mathbf{k}\cdot\mathbf{x}}, 0\right) \tag{24}$$

where ω is the angular frequency, $\mathbf{k}$ is the wavenumber and u_0 is the wave amplitude. Substituting eq. (24) into eq. (23) and using eq. (21) to calculate the forces gives

$$-4\mathrm{Sin}^2\left(\frac{\omega\Delta t}{2}\right) = \frac{\Delta t^2}{\rho}\sum_{in=1}^{N} K_{in}\left(\sqrt{(x_{in}+u_0e^{ikx_{in}+iky_{in}}-u_0)+y_{in}^2} \right. \\ \left. - |\mathbf{r}_{in}^o|\right)\cdot\mathbf{r}_{in}^t + \sum_{nim} G_{nim}\left(\frac{u_0e^{ikx_{in}} - u_o^t}{|\mathbf{r}_{in}|^2}\right), \tag{25}$$

which can be rearranged to give the dispersion equation.

$$\omega(\mathbf{k}) \\ = \frac{2}{\Delta t}\mathrm{Sin}^{-1}\left(\frac{\Delta t}{2\sqrt{\rho}}\right. \\ \left.\sqrt{-\sum_{in=1}^{N} K_{in}\left(\sqrt{(x_{in}+u_0e^{ikx_{in}+iky_{in}}-u_0)+y_{in}^2} - |\mathbf{r}_{in}^0|\right)\cdot\mathbf{r}_{in}^t + \sum_{nim} G_{nim}\left(\frac{u_0e^{ikx_{in}}-u_0^t}{|\mathbf{r}_{in}|^2}\right)}\right). \tag{26}$$

The dispersion curve is shown in Fig. 2 for a lattice where the particles were distributed on a square lattice with a length of Δx. The position of each particle was then randomly distributed about the original point inside a circle of radius $\Delta x/2$. This irregular lattice was then assigned a P-wave velocity of 3500 m s^{-1}, a S-wave velocity of 2200 m s^{-1} and a material density 2500 kg m^{-3} with $\Delta x = 10$ m and $\Delta t = 5\mathrm{e}{-4}$ s. This then implies the minimum and maximum spatial grid step was 5 and 15 m, respectively. Each particle was assigned 96 neighbours. The dispersion curve shows both the P- and S-wave. The straight line shows the non-dispersive waves. The dispersion curve shows that a dense lattice is required to sample small wavelengths adequately. The dispersion curve for the lattice method using a square grid (eight neighbours) is shown for comparison and is clearly less dispersive for a smaller number of grid points per wavelength. The effect of changing the number of neighbours is shown in Fig. 3. As the number of neighbours increases, the scheme tends to the correct P- and S-wave velocities, although the dispersion characteristics do not improve as the

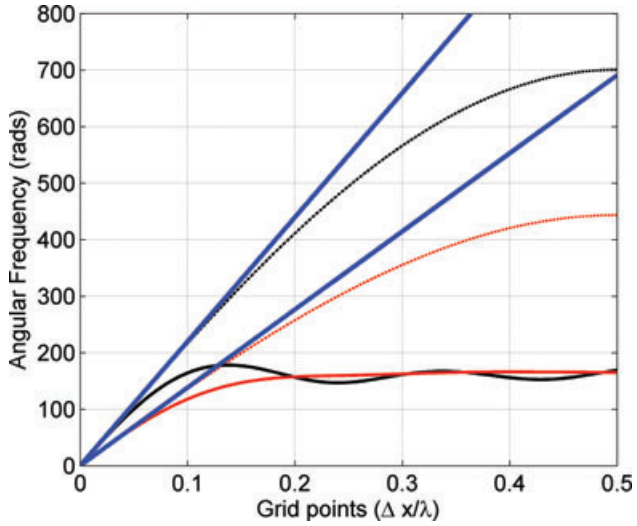

Figure 2. Dispersion curves for a square lattice method (dashed lines) and for a random lattice method with 96 nearest neighbours, see Fig. 1. The straight lines are the theoretical non-dispersive phases with the *P*-wave being the upper curve and the *S*-wave being the lower curve.

number of neighbours continually increases. The misfit between the expected phase velocities and the lattice method for a small number of particles is related to eq. (11). For a small number of neighbours, these equations do not hold and therefore the scheme does not converge to an elastic continuum. The effect of changing the time step can be assessed by comparing Fig. 4(a) and (b). The irregular lattice was generated in a similar manner to the examples above with a *P*-wave velocity of 3500 m s^{-1}, a *S*-wave velocity of 2000 m s^{-1} and a material density 2500 kg m^{-3} with $\Delta x = 10$ m. In Fig. 4(a), the time step was set to 5e−4 s and to 1e−3 s in Fig. 4(b). A smaller time step improves the dispersion properties as is expected from the regular lattice dispersion characteristics.

In Fig. 4c, the lattice structure was generated by distorting a square lattice in the same manner as above but increasing the distortion to $2\Delta x$. This leads to a more dispersive grid when comparing Fig. 4(a) and (c). This can be attributed to the fact that the maximum distance between particles has increased in certain zones, therefore to have the same dispersion characteristics larger wavelengths are required. In the final panel of Fig. 4, the *S*-wave velocity is increased to 2500 m s^{-1}. Similar behaviour to Fig. 4(a) is observed. In summary, the scheme has the same dispersion behaviour as a regular lattice method but requires a larger number of grid points per minimum wavelength. The actual number of grid points needed per minimum wavelength will depend on the required accuracy for specific problems.

4 NUMERICAL EXAMPLES

In this section, we test the accuracy of the scheme against an analytical solution and against other numerical solutions.

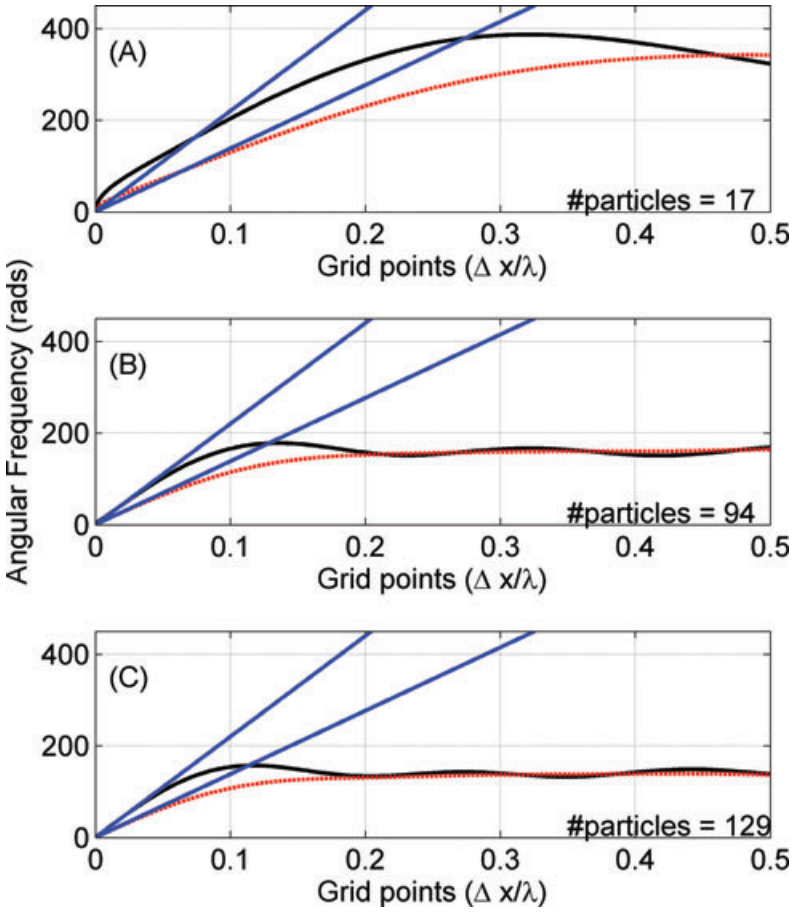

Figure 3. Dispersion curves for three different number of neighbours, (A) 17, (B) 98 and (C) 138 neighbours. The upper curves are the *P* waves and the lower curves are the *S* waves. The straight lines are the theoretical non-dispersive phases.

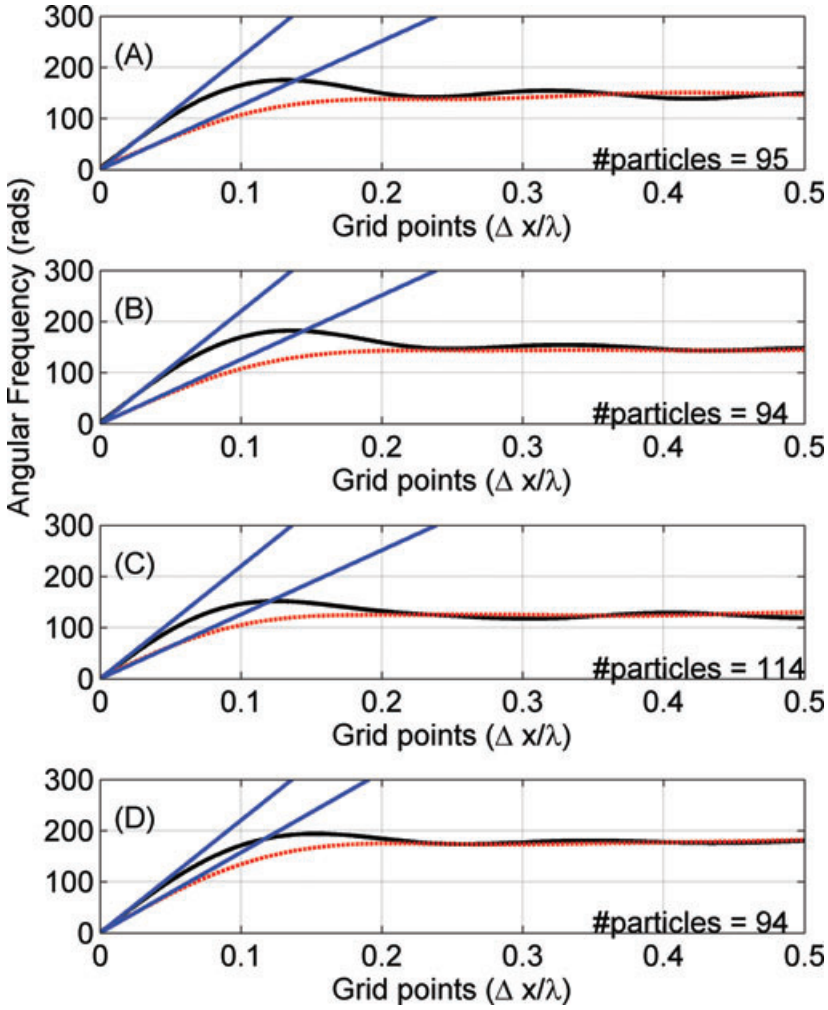

Figure 4. Dispersion curves for an irregular lattice method. (A) *P*-wave velocity of 3500 m s^{-1}, an *S*-wave velocity of 2000 m s^{-1} and a density 2500 kg m^{-3} with $\Delta x = 10$ m and $\Delta t = 5\text{e}{-4}$ s. The dispersion curve shows both the *P* and *S* waves and the straight line for non-dispersive waves. (B) The time step was set to1e−3 s with all other properties the same as (A). (C) The lattice structure was generated by distorting a square lattice in the same manner as (A) but increasing the distortion to $2\Delta x$. (D) The *S*-wave velocity is increased to 2500 m s^{-1}.

4.1 Homogeneous medium

An irregular lattice was constructed by deforming a square lattice. Each square node was randomly redistributed inside a circle centred on the original node of radius $\Delta x/2$. The *P*- and *S*-wave velocities were then set to 3500 and 2200 m s^{-1}, respectively. The density was set to 2500 kg m^{-3} and the spatial and temporal grid steps were set to $\Delta x = 10$ m and $\Delta t = 5\text{e}{-4}$ s. A 4 Hz Ricker wavelet function was used as a vertical force point source. Fig. 5 shows the vertical and horizontal wavefield after 1 s and the location of the

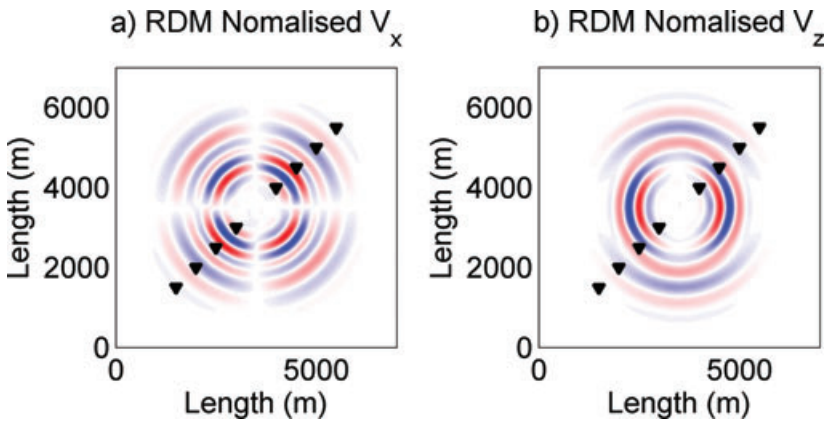

Figure 5. Vertical and horizontal velocity wavefields calculated after 1 s using the irregular lattice method in a homogeneous medium. The source was located at the centre of the model and the triangles show the location of the seismic traces in Figs 6 and 7.

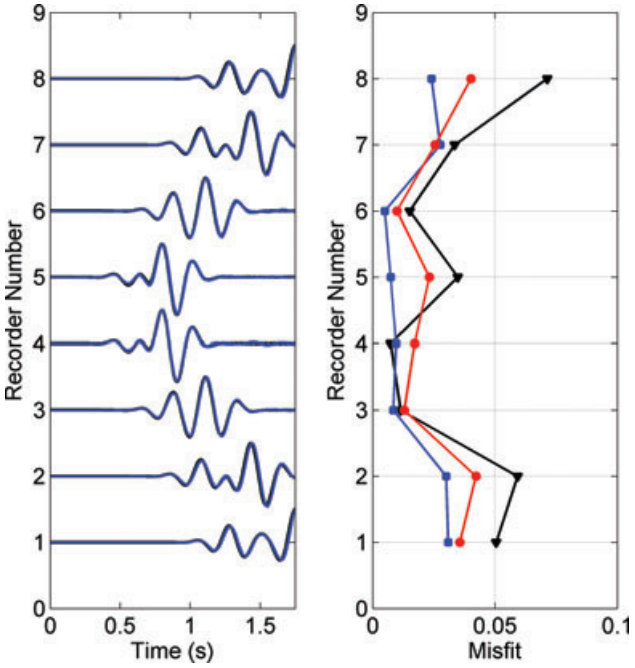

Figure 6. Analytical and numerical solution for the setup shown in Fig. 5. The recorders are labelled 1–8 moving from left to right in Fig. 5. On the left-hand panel no visible difference is observed between the analytical and numerical solution. The misfit function is shown in the right panel for numerical solutions with 64, 96 and 128 neighbours represented by triangles, squares and circles, respectively.

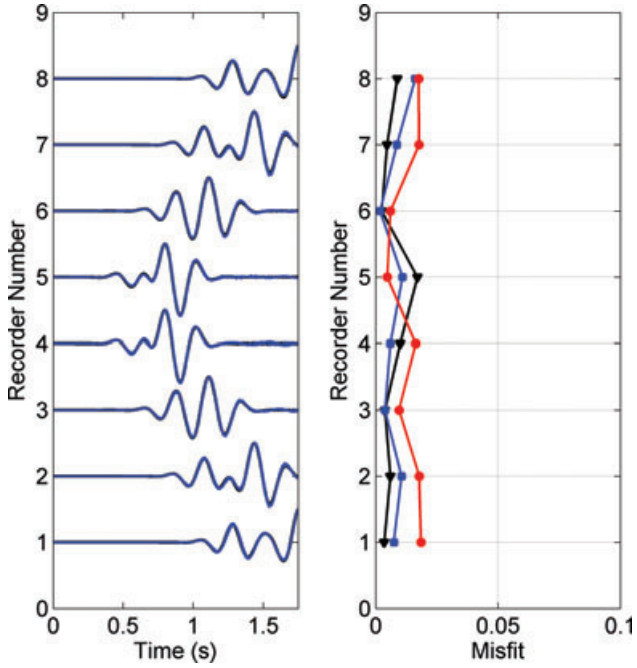

Figure 7. Comparison between a square lattice method and an irregular lattice for the setup in Fig. 5. The recorders are labelled 1–8 moving from left to right in Fig. 5. In this case, the source was input not as a point source but as a Gaussian distribution. No discernible difference between the seismograms in the left panel can be observed on the scale of the figure. The misfit function is shown in the right panel for numerical solutions with 64, 96 and 128 neighbours represented by triangles, squares and circles, respectively.

seismic recorders. The seismic traces calculated at these points were compared with an analytical solution taken from Carcione (2007) for an infinite homogenous viscoelastic medium. In this case, the Q factor was set to infinity. A comparison of the numerical and analytical solutions, along with the least squares misfit, is shown in Fig. 6. The least squares misfit is

$$\text{Misfit} = \frac{\sum_{t=0}^{T} (S^{\text{elm}}(t) - S^{\text{ref}}(t))^2}{\sum_{t=0}^{T} S^{\text{ref}}(t)^2}, \tag{27}$$

where $S^{\text{ref}}(t)$ is the reference seismogram and $S^{\text{elm}}(t)$ is the random elastic lattice seismogram.

Three different cases were compared with the analytical solution, 64 nearest neighbours, 96 nearest neighbours and 128 nearest neighbours. We found that using less than approximately 50 neighbours gave unsatisfactory results. However, this number depends on the frequency, the lattice distortion and material properties. On close inspection of Fig. 5, some residual scatter can be observed trailing the main phases. This small scale scattering is related to the source input. By inputting the source over a finite region, this scatter can be eliminated. We have done this by inputting the source over a region with a Gaussian weight using the same initial conditions as shown in Fig. 5. The seismic traces are then compared with another numerical scheme (a square elastic lattice method; Fig. 7). The misfit between these two solutions decreases relative to the previous example as the small source fluctuations are removed. In Fig. 8, we have preformed the same simulation but in a material with a different Poisson's ratio. This was done by changing the S-wave velocity to give a Poisson's ratios of 0.17, 0.25 and 0.32. From the figure it can be seen that there is little difference in the misfit.

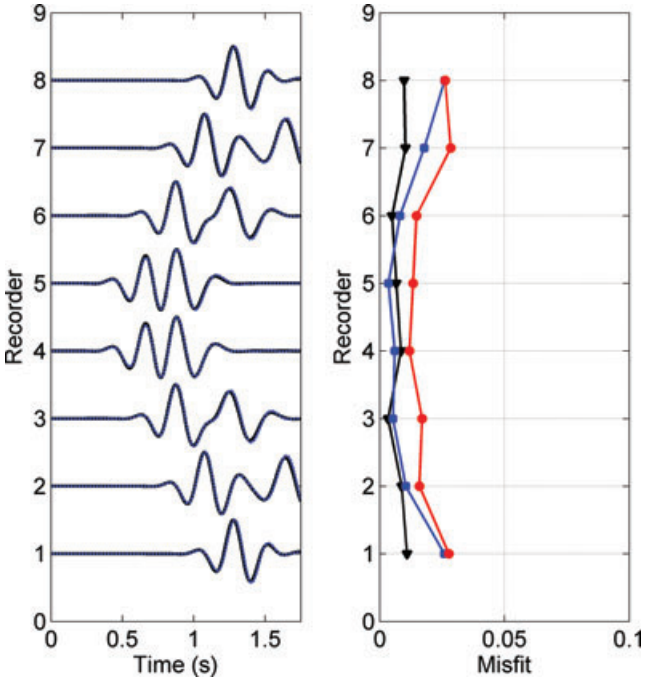

Figure 8. Comparison between a square lattice method and an irregular lattice for the setup in Fig. 5 for three different Poisson ratios. The recorders are labelled 1–8 moving from left to right in Fig. 5. The Poisson's ratio was 0.17, 0.25 and 0.32 for the triangles, squares and circles, respectively. The right panel shows the seismograms for the case where the Poisson's ratio was 0.32.

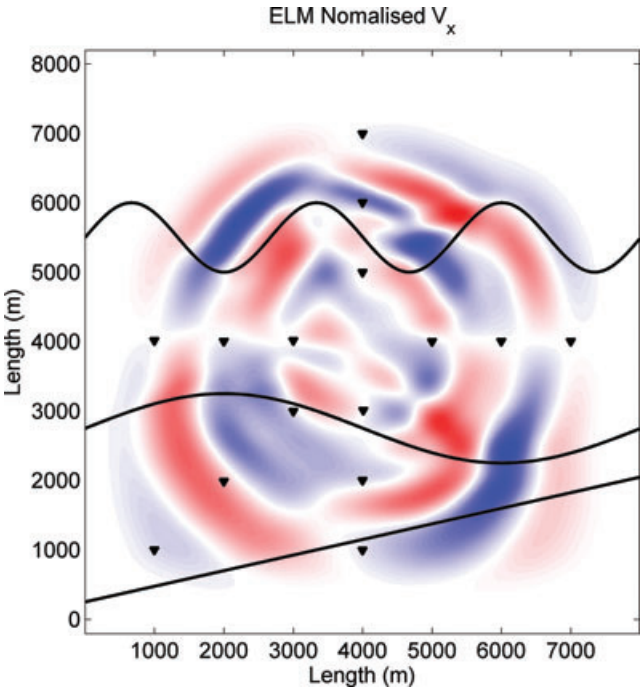

Figure 9. Horizontal wavefield calculated in a heterogeneous elastic body. The triangles show the location of the seismic traces in Fig. 10 and the solid lines show the different layers as discussed in the text. The initial *P* wavefield can be seen at the front of the wavefield but following this, individual phases can not be distinguished as the wavefield is composed of *P* and *S* waves and reflected and transmitted waves.

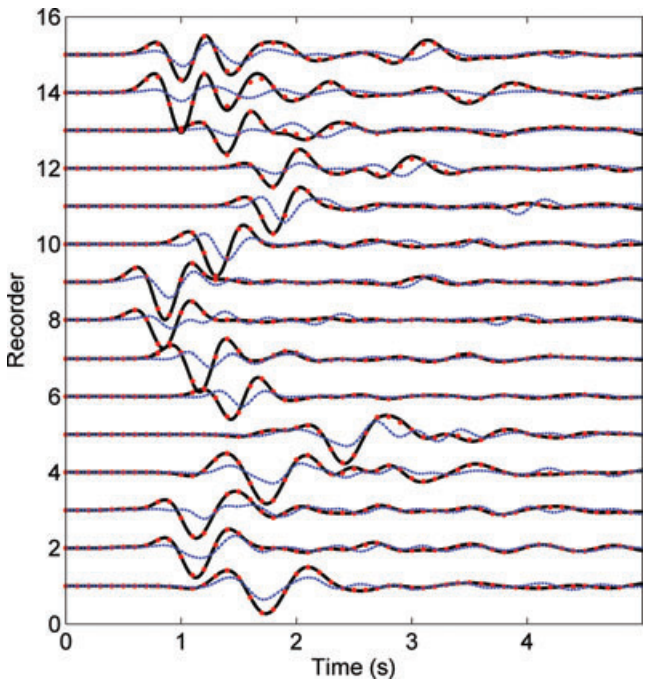

Figure 10. Seismic traces in an elastic body calculated with a regular lattice method and a spectral element method. The horizontal profile, (traces 1–5) vertical profile (traces 6–11) and diagonal profile (traces 12–15) are as shown in Fig. 9. The solid line is the SEM solution with the EL solution shown as dots. Only small differences can be observed between the two sets of seismograms. The difference between the lattice method and spectral element method is also shown as the dashed light line. The difference is scaled by a factor of 10.

4.2 Heterogeneous medium

In this case we tested the random lattice method against a numerical solution for wave propagation in a layered elastic medium. The same lattice construction was used in this case as in the previous example along with the same spatiotemporal grid steps. The material properties in the top layer were set to 2000 m s^{-1}, 1250 m s^{-1} and 2000 kg m^{-3} for the *P*-wave, *S*-wave and density, respectively. The material properties in the next layer down were set to 2500 m s^{-1}, 1500 m s^{-1} and 2300 kg m^{-3} for the *P*-wave, *S*-wave and density, respectively. The material properties in the next layer were set to 3500 m s^{-1}, 2000 m s^{-1} and 2400 kg m^{-3} for the *P*-wave, *S*-wave and density, respectively. The bottom layer had a *P*-wave of 4000 m s^{-1}, a *S*-wave velocity of 2250 m s^{-1} and a density of 2500 kg m^{-3}. We have compared the lattice solution with a solution of a spectral element code (J.-P. Ampuero, SEM2DPACK: A spectral element method for 2-D wave propagation and earthquake source dynamics, version 2.3.3, 2008). Fig. 9 shows the horizontal wavefield for the random lattice numerical solutions along with the layers and recorder locations. We have plotted several seismic traces along with the difference between the spectral element solution and lattice solution in Fig. 10. From the traces and difference, we can see that the two schemes match closely.

5 DISCUSSION AND CONCLUSIONS

Discrete particle or lattice methods are a class of numerical methods which solve the equations of motion of particles or nodes which interact through local 'microscopic' rules. The global or mesocopic behaviour of such a system can tend towards a continuum equation of state. We have presented a version of this method using an irregular lattice where a Hookean spring coupled with a bond-bending term is chosen as the local interaction rule. We have shown that by assuming linear elasticity, which underlies the elastic wave equation, the irregular lattice can behave as an isotropic elastic continuum. The system tends to an elastic continuum if a large enough number of neighbours are linked together. The geometry of the underling lattice is then removed by these long-range interactions. We have compared the method against an analytical solution for an infinite homogeneous medium and against a numerical solution for a layered medium. In both cases, the results agree well. There are two costs involved in this approach; first, including more neighbours requires more computational memory and calculations. Secondly, the dispersion analysis shows the scheme is more dispersive than a regular lattice method. This then necessitates more grid points per minimum wavelength again increasing the computing costs. The advantages of taking this approach is that (i) the material properties of the medium can be determined directly as opposed to other discrete schemes where calibration tests must be performed, (ii) the wave propagation is isotropic and not predetermined from the lattice geometry. Anisotropic wave propagation can be included by appropriate choice of the constants in eq. (7). (iii) Structural heterogeneity can be included using irregular lattices, for example curved free surfaces or faults and fractures. Because the scheme does not solve the continuum equation, the method can be used to model both static and dynamic deformation with relative ease. We would envisage the method being used for this reason and for brittle failure as opposed to pure seismic propagation where more flexible less expensive methods exist. Several crack propagation studies have been performed using this type of methodology, for example Marder &

Liu (1993), Runde (1994) and Heino & Kaski (1996). The scheme is based on simple interaction rules and fracturing can be easily included by defining a failure criterion. A stress failure criterion can be determined by calculating the stress tensor at each node or a displacement failure can be included by setting the bonds to zero once a spring is stretched or compressed beyond or under a critical length.

ACKNOWLEDGMENTS

The authors thank that this work was funded by the Department of Communications, Energy and Natural Resources under the National Geoscience Programme 2007–2013. The SFI/HEA Irish Centre for High-End Computing (ICHEC) is acknowledged for the provision of computational facilities and support.

REFERENCES

Aki, K. & Richards, P.G., 2002. *Quantitative Seismology,* University Science Books, Sausalito, CA.

Allen, M.P. & Tildesley, D.J., 1987. *Computer simulations of Liquids,* Oxford University Press, New York.

Arbabi, S. & Sahimi, M., 1988. Elastic properties of three-dimensional percolation networks with stretching and bond-bending forces. *Phys. Rev. B,* **38,** 10, 7173–7176.

Brokešová, J., 2006. *Asymptotic Ray Method in Seismology: A Tutorial*. Matfyzpress, Praha.

Carcione, J.M., 2007. *Wave fields in Real Media, Wave Propagation in Anisotropic, Anelastic, Porous and Electromagnetic Media,* Handbook of Geophysical Exploration, Vol. 38, Elsevier, Amsterdam.

Cundall, P.A. & Strack, O.D.L., 1979. A discrete numerical model for granular assemblies, *Géotechnique,* **29,** 47–65.

Del Valle-Garcia, R. & Sanchez-Sesma F.J., 2003. Rayleigh wave modelling using an elastic lattice method. *Geophys. Res. Lett.,* **30,** 16, doi: 10.1029/2003GL017600.

Heino, P. & K. Kaski, 1996. Mesoscopic model of crack branching. *Phys. Rev. B*., **54**(9), 2417–2420.

Hoover, W.G., Arhurst W.T. & Olness R.J., 1974. Two-dimensional studies of crystal stability and fluid viscosity. *J. Chem. Phys.,* **60,** 4043–4047.

Komatitsch, D. & Vilotte, J.-P., 1998. *The spectral element method: An efficient tool to simulate the seismic response of 2D and 3D geological structures*, *Bull. seism. Soc. Am.,* **88**(2), 368–392.

Landau, L.D. & Lifshitz E.M., 1986. *Theory of Elasticity,* Pergamon Press, Oxford.

Marder, M. & Liu X., 1993. Instability of lattice fracture. *Phys. Rev. Lett.,* **71**(15).

Möllhoff, M. & Bean, C.J., 2008. Validation of elastic wave measurements of rock fracture compliance using numerical discrete particle simulations. *Geophys. Prospect.,* **57**(5), 883–895, doi: 10.1111/j.1365-2478.2008.00749.x.

Monette, L. & Anderson, M.P., 1994. Elastic and fracture properties of the two-dimensional triangular and square lattices, *Modelling Simulat. Mater. Sci. Eng.,* **2,** 53–66.

O'Brien, G.S., 2008. Discrete visco-elastic lattice methods for seismic wave propagation. *Geophys. Res. Lett.,* **35,** L02302, doi:10.1029/2007GL032214.

O'Brien, G.S. & Bean, C.J., 2004. A 3D discrete numerical elastic lattice method for seismic wave propagation in heterogeneous media with topography, *Geophys. Res. Lett.,* **31**(14), L14608, doi:10.1029/2004GL020069.

O'Brien, G.S., Bean C.J., & Tapamo H., 2009. Dispersion analysis and computational efficiency of Elastic Lattice methods for seismic wave propagation, *Comput. Geosci.*, **35,** 1768–1775.

Runde, K., 1994. Dynamic instability in crack propagation, *Phys. Rev. E,* **49**(4), 2597–2600.

Toomey A. & Bean, C.J., 2000. Numerical simulation of seismic waves using a discrete particle scheme, *Geophys. J. Int.,* **141**, 595–604.

Toomey, A., Bean, C.J., & Scotti, O., 2002. Fracture properties from seismic data—a numerical investigation. *Geophys. Res. Lett.,* **29**(4), 1050, doi:10.1029/2001GL013867.

Virieux, J., 1986. P-SV wave propagation in heterogeneous media: velocity stress finite-difference method. *Geophysics* **51,** 889–901.